Numerical investigation of laminar separation in flow across elliptic cylinders

Hongyan Zhai [a, *], Zhihui Wang and Qingling Li

College of Electromechanical Engineering, Qingdao University of Science & Technology, Qingdao, China

[*, a] Corresponding author e-mail: zhaihongyan@qust.edu.cn

Abstract. This article presents the numerical studies on separate flow across elliptical cylinders of various axis ratios (AR) in the laminar region. The simulations calculated the laminar separation Reynolds number that marks separation of flow from surface and the critical Reynolds number that represents transition from steady to unsteady flow. The separate angles are expressed as the function of the axis ratio and Re in laminar region. The results are in good agreement with existing data.

1. Introduction

The phenomenon of flow separation and bluff body wakes has long been in tensely studied because of its fundamental significance in flow physics and its practical importance in aerodynamic and hydrodynamic applications. Flow behind a circular cylinder has become the canonical problem for studying such external separated flows. There have been a few experimental/numerical studies of fluid flow a from elliptical cylinders in laminar region [1,2,3]. Shih-Sheng Chen et al. [4] investigated the resonant phenomena in the wake behind a transversely vibrating elliptical cylinder with different axis ratios from AR=0.01 to AR=2.0 at Reynolds numbers 15 to 60. D. Arumuga Perumal et al. [5] studied in detail effects of blockage ratio, Reynolds number and channel length for steady and unsteady flows with lattice Boltzmann method. The simulations computed the streamline patterns at Reynolds numbers Re=3, 30, 50, 60, 100 and 150. These studies focused on the flow at finite shapes or Re. The separation parameters apply to all cases of elliptical cylinder with any AR in the laminar region are rarely mentioned in exiting literatures.

In the present work, several cases have been simulated. The geometrical and flow parameters are chosen to provide a good representation of the full parameter space.

2. Simulation methodology

2.1. Problem statement and governing equations

Consider the steady and incompressible flow of fluid with a uniform velocity V_∞ and temperature T_∞, past an elliptical cylinder of the aspect ratio, AR = b/a oriented with its long axis along the flow as shown in Figure 1 (a).. To approximate the unconfined flow conditions, the elliptical cylinder is enclosed in an imaginary concentric circular domain of diameter D as shown schematically in Figure 1 (b).

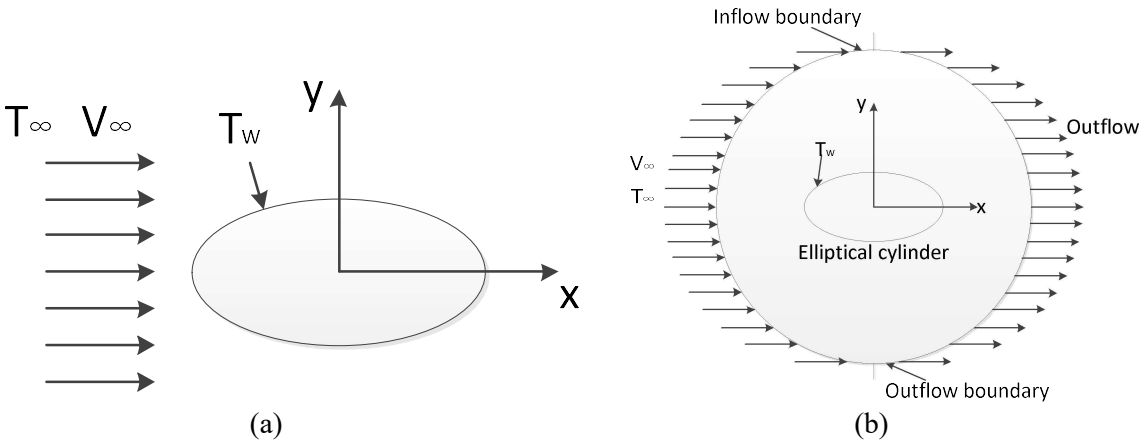

Figure 1. (a) Schematic representation of the flow (b) computational domain with boundary conditions

Flow over the cylinder is governed by the partial differential equations derived from the laws of conservation of mass, momentum and energy equation. For incompressible steady flow, the continuity and momentum equations, together with appropriate boundary conditions, are solved for velocity and pressure distributions in the domain of interest. The two-dimensional continuity equation is given by

$$\frac{\partial u}{\partial x}+\frac{\partial v}{\partial y}=0 \tag{1}$$

The momentum equation can be written as

$$u\frac{\partial u}{\partial x}+v\frac{\partial u}{\partial y}=-\frac{1}{\rho}\frac{\partial p}{\partial x}+\frac{\mu}{\rho}\left(\frac{\partial^2 u}{\partial x^2}+\frac{\partial^2 u}{\partial y^2}\right) \tag{2}$$

$$u\frac{\partial v}{\partial x}+v\frac{\partial v}{\partial y}=-\frac{1}{\rho}\frac{\partial p}{\partial y}+\frac{\mu}{\rho}\left(\frac{\partial^2 v}{\partial x^2}+\frac{\partial^2 v}{\partial y^2}\right) \tag{3}$$

And the energy equation can be expressed

$$u\frac{\partial T}{\partial x}+v\frac{\partial T}{\partial y}=\alpha\frac{\partial^2 T}{\partial y^2} \tag{4}$$

2.2. Problem statement and governing equations

To minimize the effect of the far-field boundary conditions, the circular outer boundary of the computational domain must be placed sufficiently far away from the cylinder. A computational domain extending up to a radius of 10d from the center of the computational domain was initially employed. To determine an appropriate location for the outer boundary, the computational domain was extended to 20D, 30D, 40D, 50D and 60D. In all cases, the same cell distribution was used for common subdomains. The influence of the far-field boundary on wake length, average Nu, the drag coefficient and the separation angle for a circular cylinder is given in Table 1 at Re =40. As seen from this table, moving the outer boundary from a radius of 50D–60D from the center of the cylinder does not have any noticeable effect on the flow parameters. Therefore, an annular computational domain having an outer diameter of 50D was chosen to simulate the unbounded flow past the cylinders. Zakir Faruquee et al. [6] studied the laminar fluid flow around an elliptical cylinder with the 40D domain boundary.

Table 1. Comparison of θ_S and Nu obtained using different fluid boundary sizes

domain boundary size	Wake length, L_w / D	Average Nu, Nu_{avg}	Drag coefficient, C_d	Separation angle, θ_s
20D	2.39	7.25	1.59	137.77
30D	2.30	7.20	1.56	137.77
40D	2.27	7.17	1.54	137.77
50D	2.26	7.16	1.53	137.77
60D	2.26	7.15	1.53	137.77

2.3. Mesh independence

All simulations performed in this study employed an O-type body-fitted grid system with quadrilateral cells. Grid spacing was gradually increased from the cylinder surface towards the outer boundary to avoid sudden distortion and skewness and to provide a sufficiently clustered mesh near the solid cylinder where the flow gradients are large. However, it was found that many cells were required to obtain grid independent results, especially for the rear axis velocity in the wake region.

Grid independency was achieved in this study according to the procedure outlined. Several meshes, with increasing refinement, were tested to ensure that the solution was independent of the mesh. These meshes, and the drag coefficient (C_d) and wake length (L_w) predictions are reported in Table 2 for the case of a circular cylinder at Re = 40. As can be seen from this table, a grid system with 360 nodes in the circumferential direction and 460 nodes in the radial direction under-predicts both the wake length and drag coefficient, whereas the results do not vary for meshes finer than 480×600. Thus, all results reported here are for simulations using 288,000 (360×360) cells in a computational domain with outer boundary having a radius of 50D.

Table 2. Comparison of θ_S and Nu obtained using different mesh sizes

Grid size	Minimum radial cell length near cylinder, d	Wake length, L_w / D	Average Nu, $\overline{Nu}$	Drag coefficient, C_d	Separation angle, θ_s
160×160	0.0005	2.23	7.18	1.53	138.1
360×360	0.0005	2.27	7.17	1.53	136.6
480×480	0.00001	2.27	7.16	1.53	136.8

3. Effect of axis ratio on the critical Reynolds number

The fluid around an elliptical cylinder shows the creeping flow when Re is enough small [1]. The flow begins to separate from the cylinder surface and the steady symmetric bubbles form when Re increases to Re_s. The second transition at Re_{cr} is the alternating separation of vortices with increasing Re.

3.1. The Reynolds number of separation point Re_s

Three methods of flow visualization method, wake length method [7], and flow separation criteria method [8] were used mainly in available literatures to capture the onset of separation of flow past an elliptical cylinder. This study employed wake length method to obtain Re_s. L_w/d is computed as the horizontal length between the rear stagnation point and zero velocity point in the centreline mean u-velocity profile. The results from simulations with Res 0.2, 0.4, 0.6, 0.8, 1 are shown in Figure 2. A linear fit is performed on L_w/d-Re curve to find the Re at which L_w/d becomes zero where Re is referred as Re_s. The predicted value of Res for circle cylinder in this study Re_s is 6.23. It is in good agreement with 6.27 that Immanuvel Paul et al. [7] reported, and 6.29 in S. Sen's literature [9]. Re_s with various ARs curve is exhibited in Figure 3. The functional relationships for Re_s in terms of Re and AR are proposed to obtain functional form in equation (5).

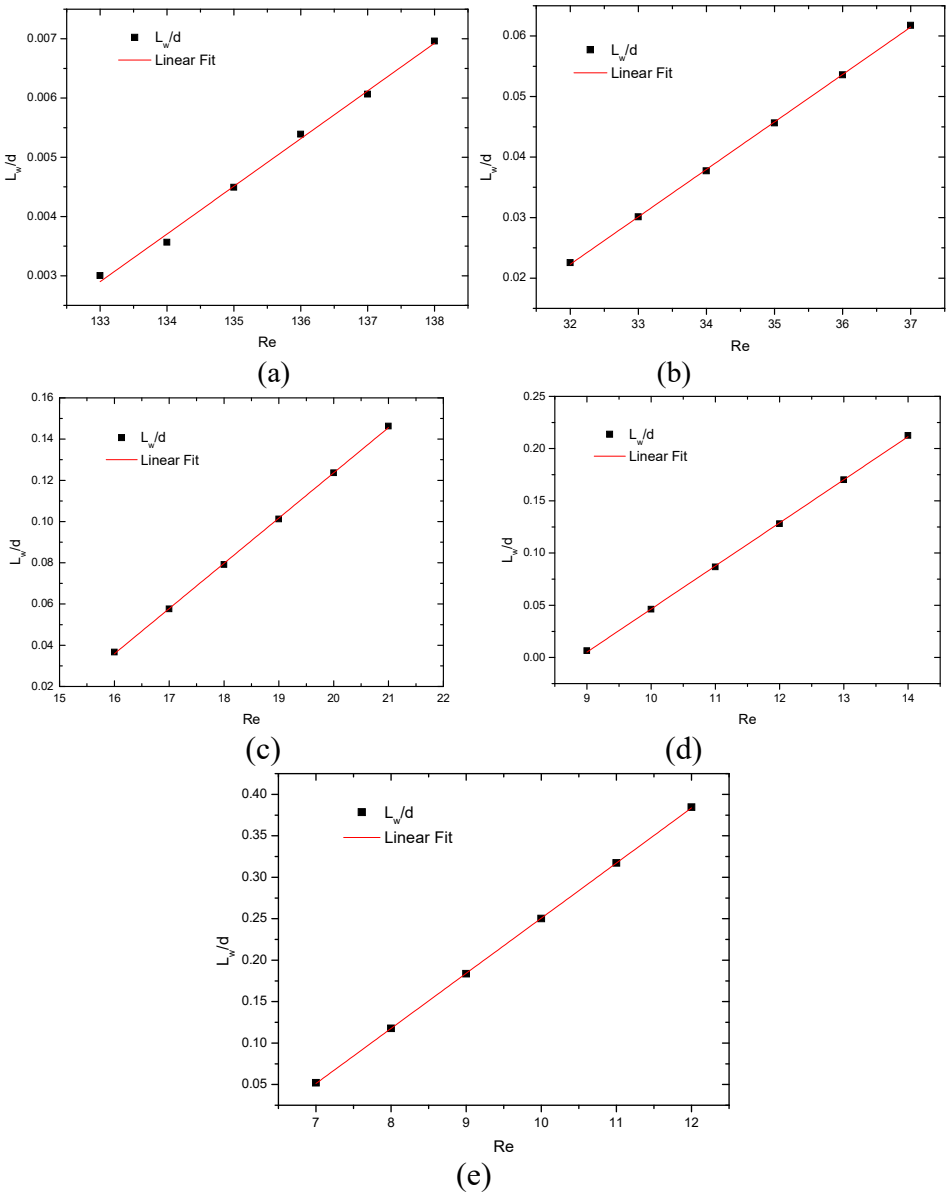

Figure 2. The values of L_w/d: (a) AR=0.2, (b) AR =0.4, (c) AR =0.6, (d) AR =0.8, (e) at AR =1.

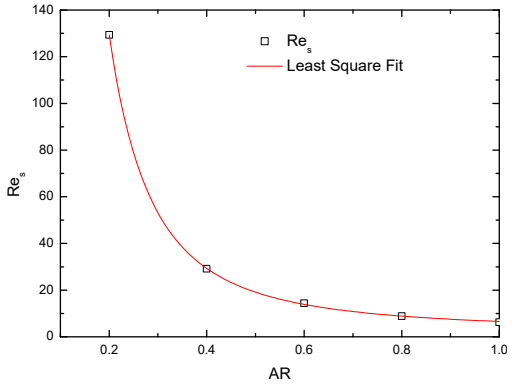

Figure 3. Re_s with elliptical cylinder with various Ars

$$Re_s = e^{0.3836+\frac{1.8063}{AR+0.2032}} \quad (5)$$

3.2. The Reynolds number of unstable flow Re_c

The stable and symmetrical vortices behind the elliptical cylinder begin to transit to the unstable state at Re_c. When the flow is stable, the amplitude of C_l with respect to time decreases. When the flow is periodic, the amplitude reaches to a saturated value. Meanwhile, C-line starts from the rear stagnation point to 10D down x-coordinate axis. Y-velocity magnitude in C-line grows from zero with unstable flow. Y-velocity magnitudes in C-line are utilized to Re_c. Simulations are initially performed for Res in steps of 1. The first Y-velocity magnitudes greater than 0 are observed at Re_c as shown if Figure 4.

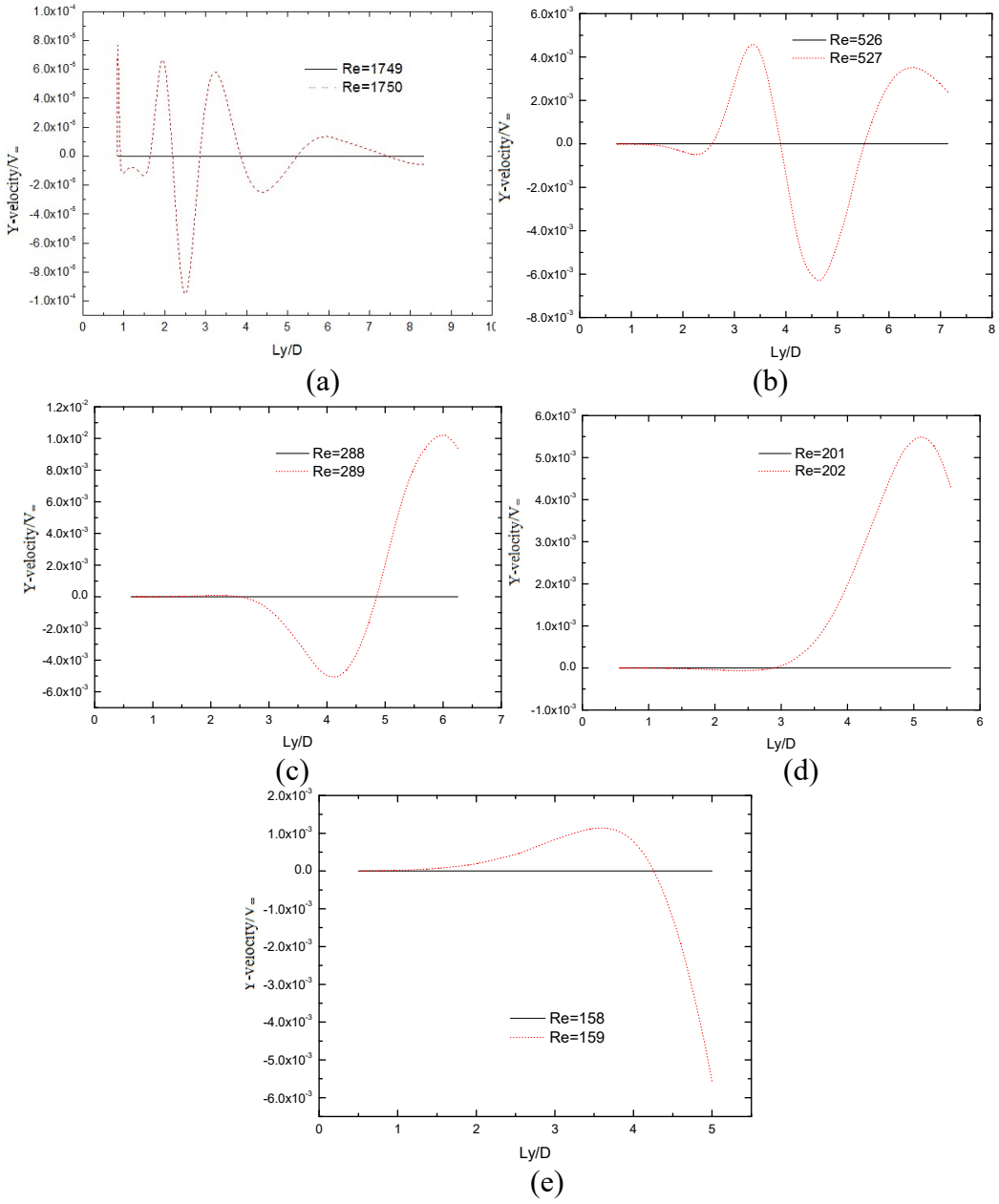

Figure 4. The Y-velocity magnitude in C-line: (a) AR=0.2, (b) AR =0.4, (c) AR =0.6, (d) AR =0.8, (e) AR =1

Recr with various ARs curve is exhibited in Figure 5. The functional relationships for Recr in terms of Re and AR are proposed to obtain functional form in equation (6).

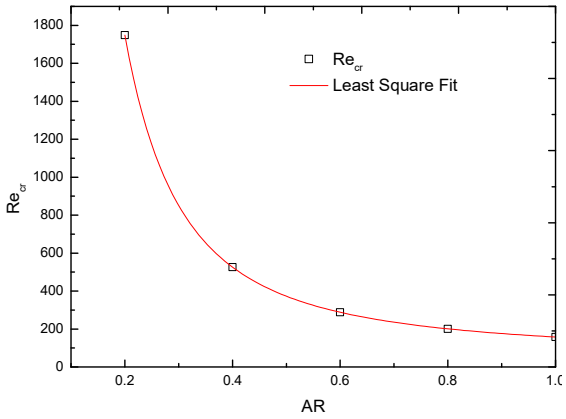

Figure 5. Re_{cr} of elliptical cylinder with various Ars

$$\mathrm{Re}_{cr} = e^{3.8577+\frac{1.4461}{AR+0.2006}} \tag{6}$$

4. Effect of axis ratio on the separation points

4.1. The separation point in the steady flow region.

The flow behind the cylinder would separate from the wall when the Reynolds is more than Re_s. The point that the separatrices separate from the cylinder surface $\tau_{\mathrm{wall}} = 0$. The flow on the sides of long axis are symmetrical. The separation angle θ_s with various ARs curve is exhibited in Figure 6. The separation point moves forward with creasing Re. $\theta_s$is greater than 90°point at the stead flow. The functional relationships for θ_s in terms of Re and AR are proposed to obtain functional form in equation (7).

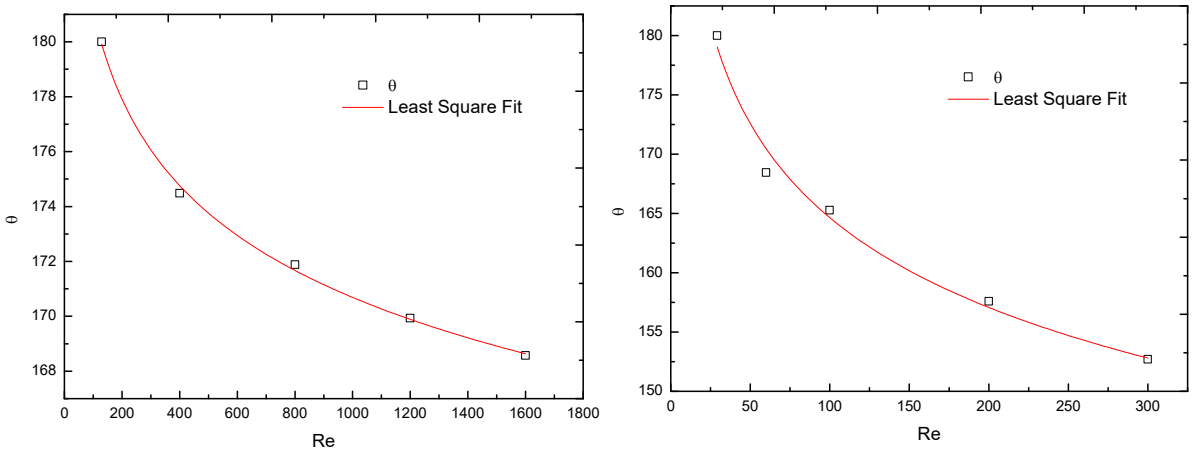

(a) (b)

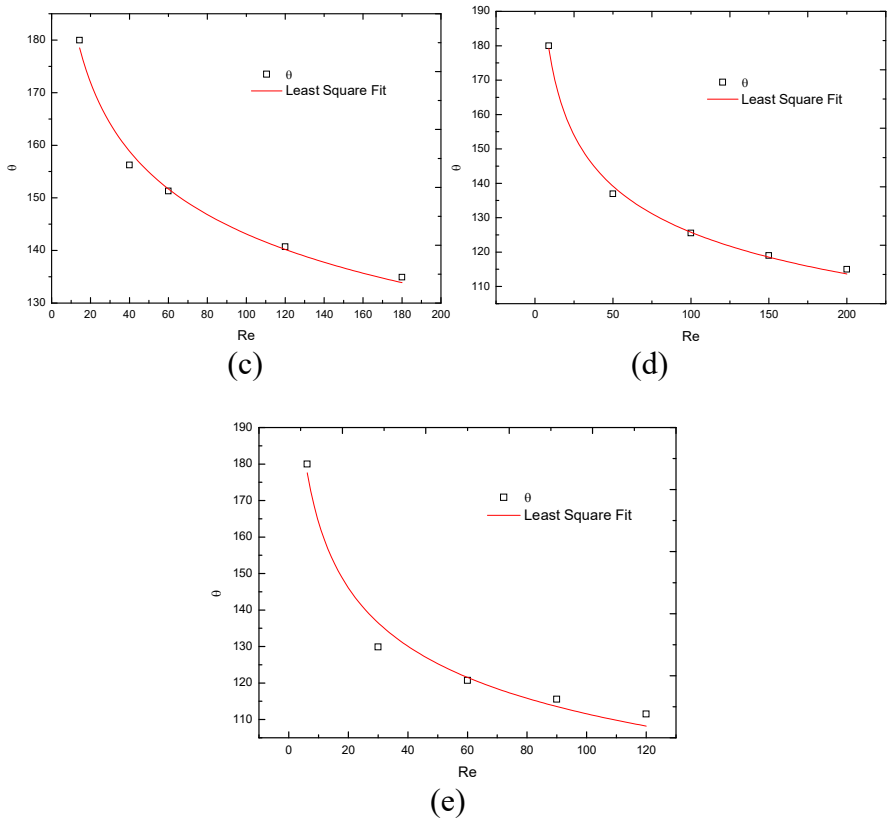

Figure 6. The separation angle when Re_s<Re<Re_{cr}: (a) AR=0.2, (b) AR =0.4, (c) AR =0.6, (d) AR =0.8, (e) AR =1

$$\theta_s = (-115.8218\mathrm{AR}^2 + 187.11352\mathrm{AR} + 170.42914)Re^{-0.17503\mathrm{AR}} \quad (7)$$

4.2. The separation point in the unsteady laminar flow region

The flow on the sides of long axis are asymmetrical when Re_s<Re<Re_{cr}, and the vorticity contours and streamlines patterns change periodically. Meanwhile, the separation point alters periodically. The streamlines and the wall shear stress at AR=0.8 and at Re=16100 are shown in Figure 7. The separation position at the same Re is the closest one in one period.

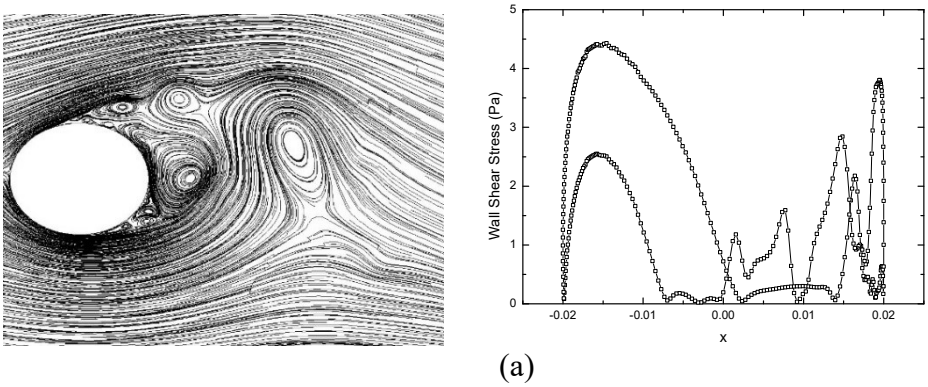

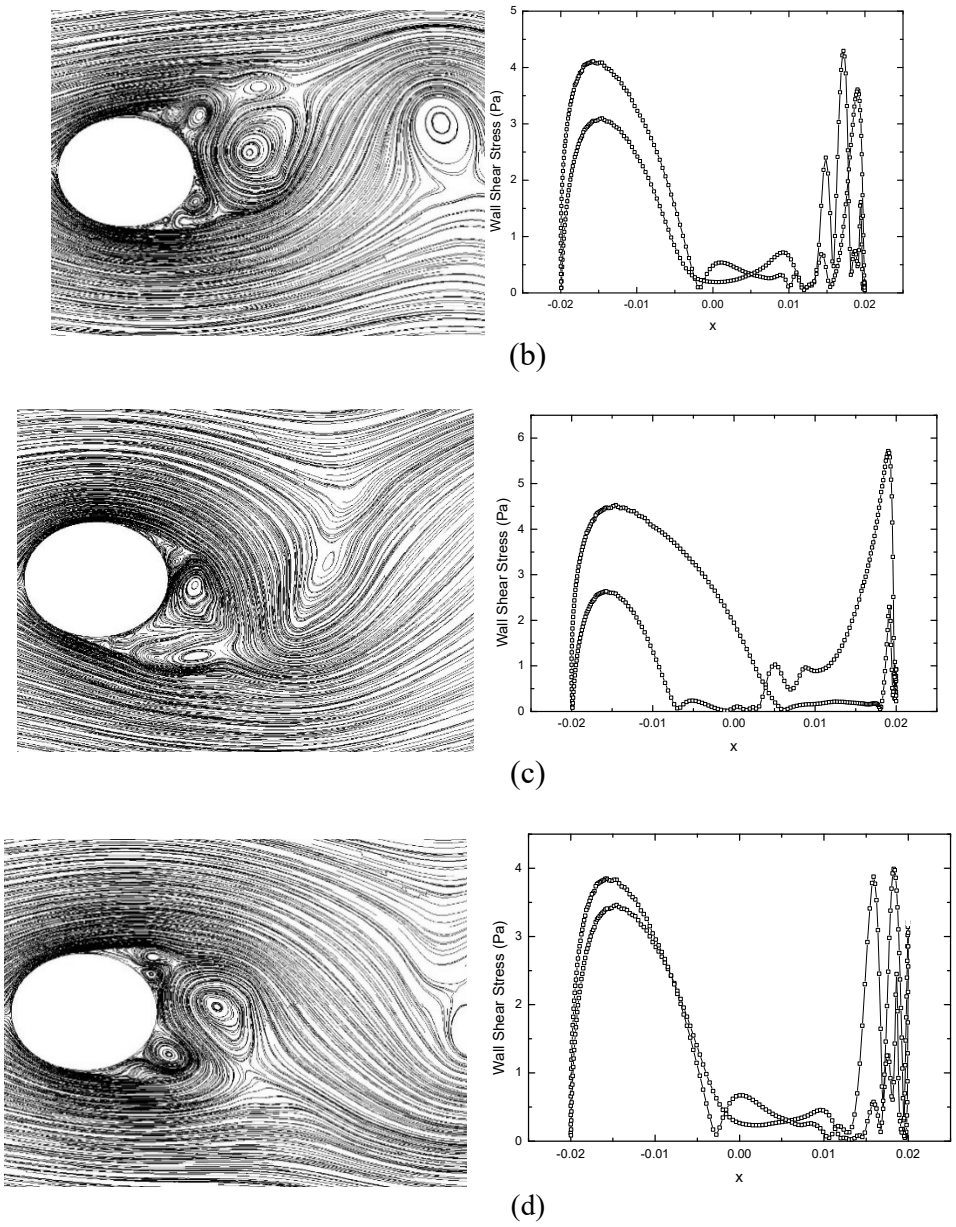

Figure 7. The streamlines and the wall shear stress at AR=0.8 : (a) t=0, (b) t=0.25T, (c) t=0.5T, (d) AR =0.75T

The separation angle $\theta_s$with various ARs curve when $Re_s<Re<Re_{cr}$ is exhibited in Figure 8. The flow separates later with smaller AR and smaller Re. The functional relationships for θ_s in terms of Re and AR are proposed to obtain functional form in equation (8).

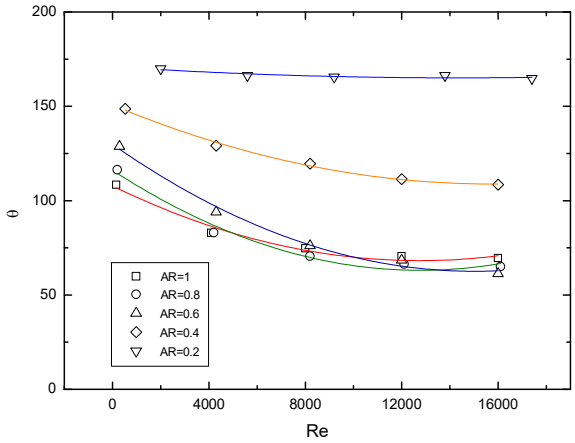

Figure 8. The separation angle on the elliptical cylinder with various ARs when Re_{cr}<Re<20000

$$\theta_s(\mathrm{AR}, \mathrm{Re}) = (-9.75609E^{-7}AR^2 + 1.46435\mathrm{E}^{-6}AR - 2.36296\mathrm{E}^{-7})Re^2 + (0.03039AR^2 - 0.04336AR + 0.00677)Re - 80.4292AR + 183.32318 \quad (8)$$

5. Conclusion

The wake of flow across an elliptical cylinder would have two transitions in laminar region at the critical Re. The fluid would separate from the wall of the cylinder when vortex arises. A number of simulation cases are worked out for separate flow. The separate angle are conclude a function about the axis ratio and Re from the numerical results. The separate point for any flow parameter would be obtained from the expression.

Acknowledgments

This work was financially supported by Shandong province's key research and development plan project of China (Grant No. 2017GGX40113), the natural science foundation of Shandong province (Grant No. ZR2017PEE001) and the plan project of Qingdao applied basic research (Grant No. 17-1-1-93-jch).

References

[1] Norman Epstein, Jacob H. Masliyah. Creeping flow through clusters of spheroids and elliptical cylinders, The Chemical Engineering Journal. (1972) 169-175.
[2] Kazuhito Shintani, Akira Umemura, Akira Takano. Low-Reynolds-number fow past an elliptic cylinder, J. Fluid Mech. 136 (1983) 277-289.
[3] R. Mittal, S. Balachandar. Direct numerical simulation of flow past elliptic cylinders, Journal of Computational Physics. 124 (1996) 351–367.
[4] Shih-Sheng Chen, Ruey-Hor Yen. Resonant phenomenon of elliptical cylinder flows in a subcritical regime, Physics of Fluids. 23(2011).
[5] D. Arumuga Perumal, Gundavarapu V.S. Kumar, Anoop K. Dass. Lattice boltzmann simulation of viscous flow past elliptical cylinder, CFD Letters. 4 (2012) 127–139.
[6] Zakir Faruquee, David S-K. Ting, Amir Fartaj, Ronald M. Barron, Rupp Carriveau. The effects of axis ratio on laminar fluid flow around an elliptical cylinder, International Journal of Heat and Fluid Flow. 28(2007) 1178-1189.
[7] Immanuvel Paul, K. Arul Prakash, S. Vengadesan. Forced convective heat transfer from unconfined isothermal and isoflux elliptic cylinders, Numerical Heat Transfer: Part Al. 64 (2013) 648-675.
[8] Kaushik Srinivasan. On a separation criterion for symmetric elliptic bluff body flows. e-print (2014) arXiv:physics/0511250[hpysics.flu-dyn].
[9] S. Sen, S. Mittal, G. Biswas. Steady separated flow past a circular cylinder at low Reynolds numbers, J. Fluid Mech. 620 (2009) 89-119.